Biochimica et Biophysica Acta 1840 (2014) 160–169

Contents lists available at ScienceDirect

Biochimica et Biophysica Acta

journal homepage: www.elsevier.com/locate/bbagen

Synthesis and toxicity characterization of carbon coated iron oxide nanoparticles with highly defined size distributions

Rafael Gregorio Mendes [a], Britta Koch [a], Alicja Bachmatiuk [a,f,g], Ahmed Aboud El-Gendy [b], Yulia Krupskaya [a], Armin Springer [c], Rüdiger Klingeler [d], Oliver Schmidt [a,e], Bernd Büchner [a], Samuel Sanchez [a], Mark Hermann Rümmeli [f,g,*]

[a] Institute for Solid State and Materials Research Dresden, Helmholtzstr. 20, 01171 Dresden, Germany
[b] Nanotechnology and Nanometrology Laboratory, National Institute for Standards (NIS), Giza, Egypt
[c] Medical Theoretical Center, Technische Universität Dresden, Fetscherstrasse 74, 01307 Dresden, Germany
[d] Kirchhoff Institute for Physics, University of Heidelberg, Im Neuenheimer Feld 227, D-69120, Heidelberg, Germany
[e] Material Systems for Nanoelectronics, Chemnitz University of Technology, Reichenhainer Str. 70, 09107 Chemnitz, Germany
[f] IBS Center for Integrated Nanostructure Physics, Institute for Basic Science (IBS), Daejon 305-701, Republic of Korea
[g] Department of Energy Science, Sungkyunkwan University, Suwon 440-746, Republic of Korea

ARTICLE INFO

Article history:
Received 20 January 2013
Received in revised form 16 August 2013
Accepted 27 August 2013
Available online 3 September 2013

Keywords:
Iron oxide nanoparticle
Carbon coating
Cancer cell
(3-[4,5-dimethylthiazol-2-yl]
-2,5-diphenyltetrazolium bromide) assay
Trypan blue assay
Nanotoxicity

ABSTRACT

Background: Iron oxide nanoparticles hold great promise for future biomedical applications. To this end numerous studies on iron oxide nanoparticles have been conducted. One aspect these studies reveal is that nanoparticle size and shape can trigger different cellular responses through endocytic pathways, cell viability and early apoptosis. However, systematic studies investigating the size dependence of iron oxide nanoparticles with highly defined diameters across multiple cells lines are not available yet.
Methods: Iron oxide nanoparticles with well-defined size distributions were prepared. All samples were thoroughly characterized and the cytotoxicity for four standard cell lines (HeLa Kyoto, human osteosarcoma (U2OS), mouse fibroblasts (NIH 3T3) and mouse macrophages (J7442)) where investigated.
Results: Our findings show that small differences in size distribution (ca. 10 nm) of iron oxide nanoparticles do not influence cytotoxicity, while uptake is size dependent. Cytotoxicity is dose-dependent. Broad distributions of nanoparticles are more easily internalized as compared to the narrow distributions for two of the cell lines tested (HeLa Kyoto and mouse macrophages (J7442)).
Conclusion: The data indicate that it is not feasible to probe changes in cytotoxicity within a small size range (10 nm). However, TEM investigations of the nanoparticles indicate that cellular uptake is size dependent.
General significance: The present work compares narrow and broad distributions for various samples of carbon-coated iron oxide nanoparticles. The data highlights that cells differentiate between nanoparticle sizes as indicated by differences in cellular uptake. This information provides valuable knowledge to better understand the interaction of nanoparticles and cells.

1. Introduction

Magnetic nanoparticles are of great interest for use in a wide range of disciplines and are expected to play an evermore important role in biotechnology and biomedicine. Novel methods in treatment and diagnostics are being developed using nanoparticles (NPs) with the promise of overcoming many of the limitations of current procedures. Nonetheless, dextran coated iron oxide nano-particles are the only form of NPs thus far approved by the US Food and Drug Administration (FDA). The interest in iron oxide NPs lies in their potential as elements for contrast enhancement in magnetic resonance imaging, tissue repair, immunoassay, detoxification of biological fluids, cell separation, drug delivery and hyperthermia [1–7].

The scientific curiosity with regard to nanoparticles stems from their size dependent-properties that mainly originate from the dominance of their large surface area. Moreover, the morphology of NPs can be an intrinsic functionalization in itself [8]. However, the impact of the size and shape of NPs on their toxicological effects is only beginning to be investigated and its understanding is crucial for designing their physical and chemical properties more accurately and according to the requirements. Stoehr et al. [9] found that spherical silver nano- and microparticles exhibit little impact on alveolar epithelial cells whereas wire-shaped silver particles induced a strong cytotoxicity, loss in cell viability, and early calcium influx. Another recent study with silica NPs showed that

* Corresponding author at: Institute for Solid State and Materials Research Dresden, Helmholtzstr. 20, 01171, Dresden, Germany. Tel.: +49 82312994055.
E-mail address: mhr1@skku.edu (M.H. Rümmeli).

0304-4165/$ – see front matter © 2013 Elsevier B.V. All rights reserved.
http://dx.doi.org/10.1016/j.bbagen.2013.08.025

variations in their shape and size can trigger different cellular responses and even influence the cell migration on surfaces [10]. Various other studies hint that NP size and shape can trigger different cellular responses in endocytic pathways, cell viability and early apoptosis [11–14]. Theoretical and experimental studies with iron oxide NPs with large diameter distributions suggest that particles of different diameters could be internalized differently by cells which could lead to different biological responses. However, the mechanisms involved are still unclear [15]. Ying and Hwang investigated the cytotoxicity of iron oxide NPs with different sizes and coatings on A3 human T lymphocytes using commercial NPs for which no information on their diameter distributions was available [16]. Another study compared various metal oxide particles including iron oxide, again using only a single cell line. The diameter distributions of the investigated NPs were very large [17]. Ideally studies with very narrow diameter distributions, so called monodisperse samples, are thought to be preferable so as to avoid any size dependency that may or may not exist within the observed diameter distribution.

To our knowledge no systematic study on size dependency of cytotoxicity using iron oxide NPs with highly defined diameter distributions across multiple cell lines exists so far. Even though iron oxide NPs are regarded as stable [18], there is the risk that NPs in general can react when in direct contact with an external biological environment. This can lead to their degradation resulting in toxic byproducts [19]. A promising means to overcome this problem is to use coatings that can also provide these particles with new and enhanced properties [20]. Some examples include polymers [21,22], surfactants [23] and proteins [24]. A recent study suggests that it is not only the type of molecule used in the bioconjugation that is important, but also how it is distributed on the surface [25]. Even differences in the surface charge of NPs can be recognized by cells [26]. Carbon coatings are attractive because they do not only offer high chemical and thermal stability, but also provide a platform that can be easily functionalized [27–30]. In the case of magnetic NPs (e.g. iron oxide), carbon coatings can also help to reduce magnetic interparticle interactions and thereby hinder agglomeration [31]. Indeed carbon-based nanostructures are potentially attractive for a variety of applications in biomedicine ranging from drug delivery to biosensing [32–36].

There are an increasing number of publications relating the cytotoxicity levels of nanoparticles to their morphology with special emphasis on size, shape, and surface defects. However this correlation between morphology and cytotoxicity has been mostly investigated for nanoparticles pursuing extreme differences such as comparing 10 nm particles with 100 nm ones or using samples that do not have a homogeneous nature (e.g. different shapes and sizes intermixed within a sample). Here we deliberately focus on a small range of diameters and narrow specific diameter distributions of purely spherical iron oxide nanoparticles. To our knowledge there is still a need to determine if cells are able to discriminate between small diameter variations in the order of 10 nm, namely when differences in the size of NPs start to be significant and measurable when brought together with cells. In this work we aim to investigate a small range of diameters of iron oxide NPs. For this we use a colloidal chemistry route involving the decomposition of iron oleate to synthesize spherical iron oxide NPs [37]. Moreover, the technique inherently leaves a thin carbon rich coating on the surface of the as-produced NPs. The implemented synthesis route is attractive because, apart from yielding NPs with highly defined diameter distributions, it is also possible to tailor the mean diameters of the NPs by varying the reaction conditions. We also show that one can tailor the width of the diameter distribution by altering the purity of the precursors. This allowed us to produce three very narrow size distributions (9.7, 14.8 and 16.8 nm) and full width at half maximum (FWHM) corresponding to 1.4 nm, 1.4 nm, 2.5 nm, respectively. In addition, a fourth sample with a broad diameter distribution (20.3 nm) and FWHM of 5.5 nm spanning the diameters of the initial three samples was prepared. The results are presented in Table 1. These samples enable us to investigate two important questions. Firstly, are the cytotoxicity and cellular uptake influenced by small diameter changes and secondly, are the cytotoxicity and uptake sensitive to broad diameter distributions as compared to narrow diameter distributions? This latter question is important when considering the synthesis of high performance NPs on an industrial scale where a broad diameter distribution usually implies reduced production costs.

The as-produced samples were carefully characterized and their biocompatibility was evaluated. In order to determine the material toxicity and the possible size dependence, four cell lines were incubated with the NPs and the cell viability was measured using the MTT and trypan blue assays. The standard cell lines used in the viability assays were HeLa Kyoto, human osteosarcoma (U2OS), mouse fibroblasts (NIH 3T3) and mouse macrophages (J7442).

2. Experimental

2.1. Iron oxide NP synthesis

The iron oxide NPs were synthesized based on the work of L. M. Bronstein [38], which is now briefly explained. A typical procedure to synthesize iron oxide NPs with highly defined sizes is based on the iron oleate complex serving as a precursor. This complex is formed in the reaction between iron chloride (III) and sodium oleate dissolved in a mixture of ethanol, hexane and distilled water. When heated for 4 h on a hot plate, the metal chloride and the sodium oleate react to form a metal–oleate complex (iron oleate) and sodium chloride (NaCl). The resulting mixture containing the iron oleate is then washed with distilled water to remove the salt byproduct and the oleate is isolated using a separation funnel. The purified and waxy complex is then thermally decomposed by boiling in a high temperature solvent. Following a modified procedure of the original synthesis route [38], the iron oleate complex passes through a two-step process, which allows the formation of NPs with different diameters. As a first step the iron oleate complex is thermally treated in vacuum for 24 h at 30 and subsequently 70 °C. This heating treatment removes crystal hydrate water and at 70 °C dissociates the metal carboxylate bonds [38]. The second step is the thermal decomposition of the iron oleate complex in different solvents. The use of various solvents to decompose the iron oleate complex is important because each solvent has a different boiling temperature at which the decomposition occurs and plays a role in the final monodispersed size of the NPs. In other words the different temperatures influence the nucleation and growth processes of the NPs. The different thermally treated iron-oleate complexes were firstly dissolved in a mixture of oleic acid and different solvents (octadecane, octadecene, eicosane and docosane) and heated up for different periods of time and temperature in a reflux system. The solution, which then contains the iron

Table 1
Main parameters used to synthesized different size iron oxide nano-particles and comparison between LVTEM mean diameter evaluations and diameter estimates using the Scherrer equation.

Sample	Anneal in vac. [°C]	Solvent	Reflux temp. [°C]	Reflux time [min]	TEM diameter [nm]	Scherrer size [nm]	Full width at half maximum [nm]
a	30	Octadecane	318	30	9.7 (±1.4)	12.3 (±4.5)	1.4
b	70	Docosane	365	3	14.8 (±0.8)	14.3 (±4.8)	1.4
c	70	Eicosane	335	30	16.8 (±1.4)	16.7 (±5.3)	2.5
d	–	Octadecene	300	30	20.3 (±2.6)	18.3 (±9.2)	5.5

oxide crystals, is afterwards cooled down to room temperature. Ethanol and acetone were used to precipitate the crystals, which were collected using a strong magnet. Moreover all samples were intensely rinsed with organic solvents (chloroform and hexane) and again collected using a strong magnet. This process was used to remove possible remnants from the oleic acid, avoiding in this way an unwanted coating oleic acid on the NPs. Table 1 provides a summary of the as-synthesized NPs and the decomposing solvent used. It is important to mention that the iron oleate complex used in the synthesis of the sample containing the NPs with an average diameter of 20.3 nm was not annealed in vacuum and used precursor chemicals with different impurity contents, which led to the formation of a broad size distribution.

The commercial chemicals $FeCl_3.6H_2O$ (98%), docosane (99%), eicosane (99%), octadecane (99%) and octadecene (99%) were purchased from Alfa Aesar. Hexane, ethanol, chloroform, acetone and oleic acid were purchased from Merck Chemicals. The sample containing the iron oxide nanoparticles with the broad size distribution (Sample D) was synthesized using the sodium oleate purchased from Sigma Aldrich with a purity of 82%, whereas the other samples with narrow distributions were synthesized with a sodium oleate purchased from J. T. Baker with a higher purity (90–100%).

The as-produced material was analyzed using a transmission electron microscope (TEM model JEOL 2010F), X-ray diffraction apparatus (Rigaku Miniflex), a Raman spectrometer (Thermo Scientific DXR) and a Fourier transform infrared spectrometer (Bruker).

2.2. Biological studies

2.2.1. Cell culture

HeLa cells (Kyoto line) were cultured in DMEM + GlutaMAX™ (gibco) supplemented with 1% NEAA (gibco); human osteosarcoma U2OS cells (GFP-53BP1) in standard DMEM (Sigma-Aldrich) supplemented with 1 mM pyruvate and 0.5 mg/mL genectin (gibco) and NIH 3T3 mouse fibroblast as well as macrophage J7442 cells were grown in DMEM F12HAM supplemented with 2 mM L-glutamine (Sigma-Aldrich). Additionally all the media contained 10% FBS (Sigma-Aldrich), 100 U/mL penicillin and 100 μg/mL streptomycin (gibco). To create a cell suspension the cells were washed once with PBS (gibco) and detached using a cell scraper for the macrophages (Greiner Bio-One) or for the other cell lines, 0.25% Trypsin–EDTA solution (Sigma).

2.2.2. MTT viability assay

For cell viability studies, a commercial TOX-1 in vitro toxicology assay kit (Sigma-Aldrich) was used. The assay measures the viability of living cells via the cleavage of MTT (3-[4,5-dimethylthiazol-2-yl]-2,5-diphenyltetrazolium bromide) to purple formazan crystals by the cells' mitochondrial dehydrogenases. Four different cell lines were grown in standard 96 well flat-bottom plates as testing systems and 4.0×10^5 cells per well were tested. The NPs were suspended in DI water at a stock concentration of 0.5 mg/mL. To assure a uniform dispersion of the particles the suspensions were vortexed (stirred) on a Vortex Genie 2 T for 2 min prior to usage. After incubating the cells at 37 °C and 5% CO_2 in the presence of increasing concentrations of NPs (controls with only DI water, 1 μg/mL, 10 μg/mL and 100 μg/mL) for either 12 or 48 h, 10 μL of the MTT solution (5 mg/mL in PBS) was added to the 0.1 mL culture medium per well and the 96 well plates were returned to the incubator for another 4 h. After carefully removing 80 μL of the supernatant the produced formazan crystals were then dissolved in 0.1 mL of the prewarmed MTT Solubilization Solution (10% Triton X-100, 0.1 N HCl in anhydrous isopropanol) by gently shaking the plates in an ELISA microplate reader (15 min, 14 Hz, 37 °C, SAFAS MP96). The absorbance of the formazan dye was measured in the SAFASMP96 reader at 550 nm/650 nm within an hour and after having subtracted the background from the sample, the percentage cell viability was calculated. Each of the conducted experiments was repeated three times.

2.2.3. Dye exclusion test (trypan blue)

The cell lines were grown in standard 6 well flat-bottom plates and incubated for 12 or 48 h with the respective nanoparticle suspension at a concentration of 10 μg/mL. Afterwards the cells were detached and resuspended in 1 mL cell culture medium per well. 20 μL of each cell suspension was carefully mixed with 0.4% trypan blue solution (Sigma) and added to the chambers of a standard hemocytometer (improved Neubauer) to count the number of viable and dead cells. The results are presented as means of two measurements each and their deviation.

2.2.4. Live cell imaging

Cells were cultured in 6 well plates. Images were acquired with an Axio Observer Z1 inverse microscope equipped with a 37 °C heated stage and CO_2 chamber. The software Axio Vision Rel. 4.8 (Carl Zeiss, Inc.) was used for the image acquisition.

2.3. TEM studies

The cells were grown in a 10 cm petri dish as described above and incubated with the NPs in a concentration of 10 μg/mL for a period of 12 h and 48 h respectively. After collecting the cells from the culture dish and centrifugation at 1000 rpm for 5 min, the supernatant was removed. The cell pellets were fixed in a 2.5% glutaraldehyde solution in PBS for 4 h. They were then rinsed with PBS, embedded in a 4% agarose gel, stained in a 2% osmium tetroxide solution for 24 h and then rinsed with distilled water. The samples were then additionally stained with 1% uranyl acetate for 1.5 h, dehydrated in a graded series of acetone (25, 50, 75, 96 and 100%), and then embedded in an epoxy resin. The resin was polymerized first for 3 h at 50 °C and then the temperature was increased to 60 °C for 48 h. Ultrathin sections (50–70 nm) were obtained with an ultramicrotome and imaged using a transmission electron microscope (TEM) model JEOL 2010F retrofitted with two third order Cs aberration correctors from CEOS operating at 80 kV and a FEI TECNAI T20 operating at 200 kV.

2.4. Sample characterization

The morphological characterization (shape, diameter and coating) of the samples was conducted using a TEM. The samples were dispersed in a non-polar solvent and a 5 μL droplet at a concentration of approximately 1 mg/mL was placed and dried on a carbon film coated TEM grid. The crystalline structure of the samples was analyzed using an X-ray diffractometer (XRD) (model Rigaku Miniflex). The XRD pattern was used to estimate the average crystal size and the results were compared with the TEM observations. The presence of sp^2-carbon was studied using Raman spectroscopy (model Thermo Scientific DXR, laser $\lambda =$ 532 nm). To examine the different NP samples they were pressed and fixed on Si/SiO_2 wafers prior to the measurement. The as-produced samples were dried and small amounts of the powder were weighted before both the magnetization over external field (MxB) and temperature (MxT) were conducted in a VSM-SQUID from Quantum Design. The heating experiments were performed in purpose built equipment with an operating frequency of 120 Hz. The samples were dispersed in an aqueous solution using a tip sonicator with a concentration of 5 mg/mL and measured over 4 min.

3. Results

3.1. Sample characterization

The morphology of the as-synthesized iron oxide NPs was studied using low voltage transmission electron microscopy (LVTEM) at 80 kV. In Fig. 1 ordered arrays of iron oxide NPs formed on carbon membrane TEM grids are shown. The images, as well as in-depth statistical analysis of the particles, reveals that the NPs presented in Fig. 1 panels A, B and C

have highly narrow diameter distributions and all consist of spherical particles, whereas the NPs in Fig. 1 panel D have a variation in size and shape. The broader distribution varies from 10 to 26 nm and envelopes the sum of the 3 narrow diameter distribution samples. Both spherical and cubic NPs can be observed in the samples shown in panel D of Fig. 1. A statistical analysis was conducted for at least 100 particles with each particle's diameter measured at four positions and then averaged.

High resolution LVTEM investigations show that the iron oxide NPs are single crystals and have a graphitic coating. Panels A and B of Fig. 2 show two typical examples of crystalline iron oxide NPs. The surface of the NPs has a layered structure (see arrows) hinting at a graphitic coating. Typically the coating thickness is 0.5–1.0 nm, which corresponds to 1–3 graphitic layers. To investigate the coating in more detail we employed Raman spectroscopy. This technique is sensitive to sp^2 carbon materials, in particular to the presence of the so called G mode (ca. 1600 cm^{-1}), which appears due to bond stretching of all sp^2 carbon pairs in both rings and chains, and the D mode (ca. 1350 cm^{-1}), which is due to the fact that breathing modes of sp^2 atoms in rings can provide signatures for the presence of graphitic material [39]. Fig. 2C shows a typical Raman spectrum in which both the G and D modes are present. The modes are broad and the D mode, which is activated by defects, is rather large. These factors indicate a rather defective graphitic material. The carbon coating probably consists of defective turbostratic graphene-like layers. Despite the fact that the exact mechanisms involved in the formation of these thin graphene-like layers are not investigated in more detail, they are likely formed during the decomposition process due to the high temperatures used. The energy dispersive X-ray spectroscopic (EDS) studies show only the presence of carbon (C), oxygen (O) and iron (Fe) indicating that the as-produced iron oxide NPs coated with carbon are pure. Additionally Fourier transform infra-red (FTIR) studies were conducted to better investigate the NP surface coating. A typical example is shown in Fig. 2D. The absorbance spectrum of oleic acid (precursor material) is provided for comparison. The FTIR data show a variety of functional groups, namely, a C–O bond with a peak at 805 cm^{-1}, a bending mode peak of C–C can be seen at 1050 cm^{-1}, a C═O bond with a peak close to 1700 cm^{-1} and C–H and O–H bonds are present at higher wavenumber values above 2500 cm^{-1}. The strong peak appearing at 550 cm^{-1} is assigned to ferrite. The presence of these groups contributes to the dispersion of the NPs in aqueous solution after ultrasonication. However it cannot be excluded that traces of oleic acid may also be present. The existence of oleic acid has been observed in other samples produced from this synthesis route, however, this molecule is not toxic and can itself form a platform for further functionalization [40].

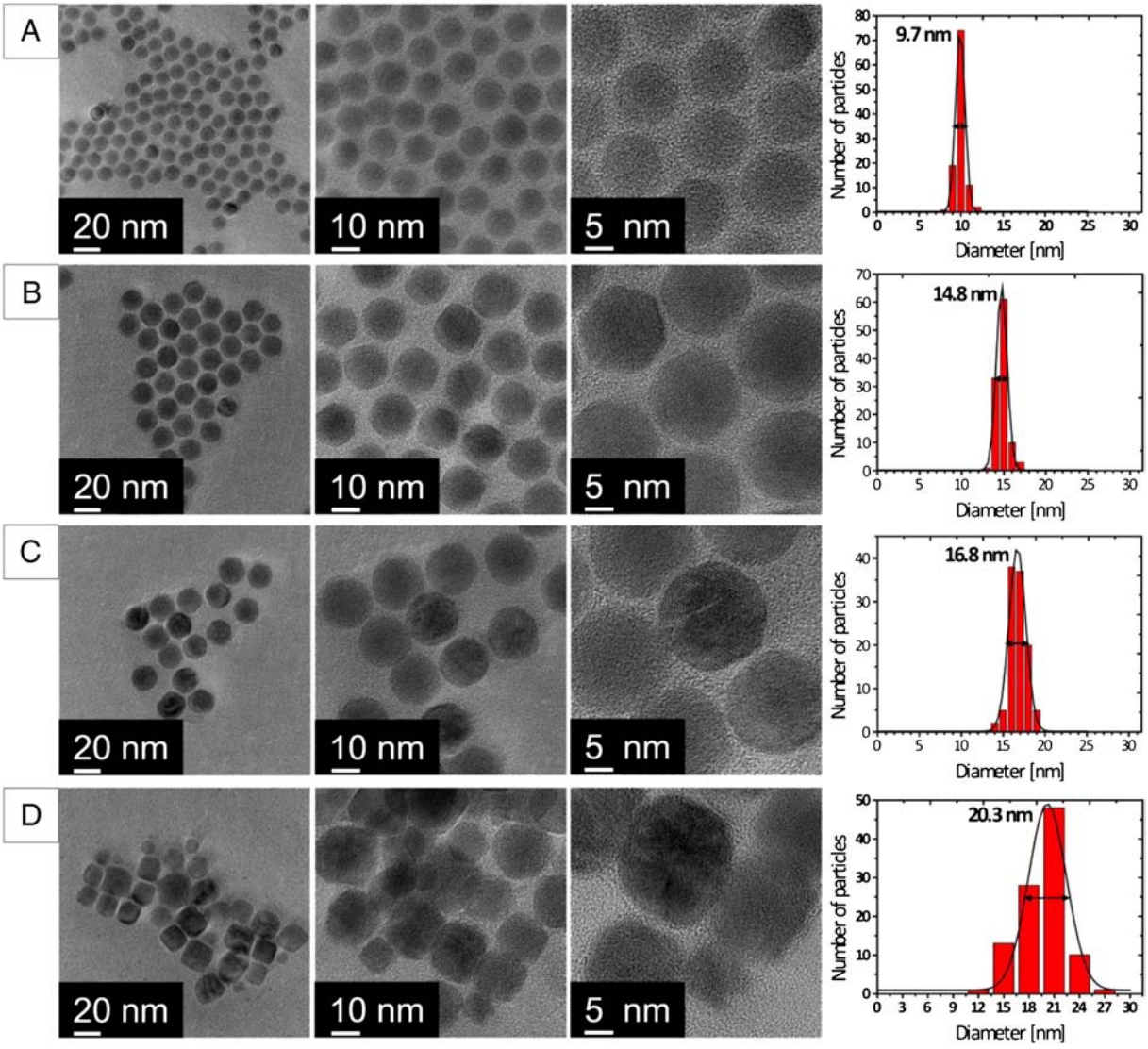

Fig. 1. TEM images showing the four as-produced samples. Panels A, B and C show the NPs that have narrow diameter distributions while panel D has a broad diameter distribution that envelopes the sum of A, B and C.

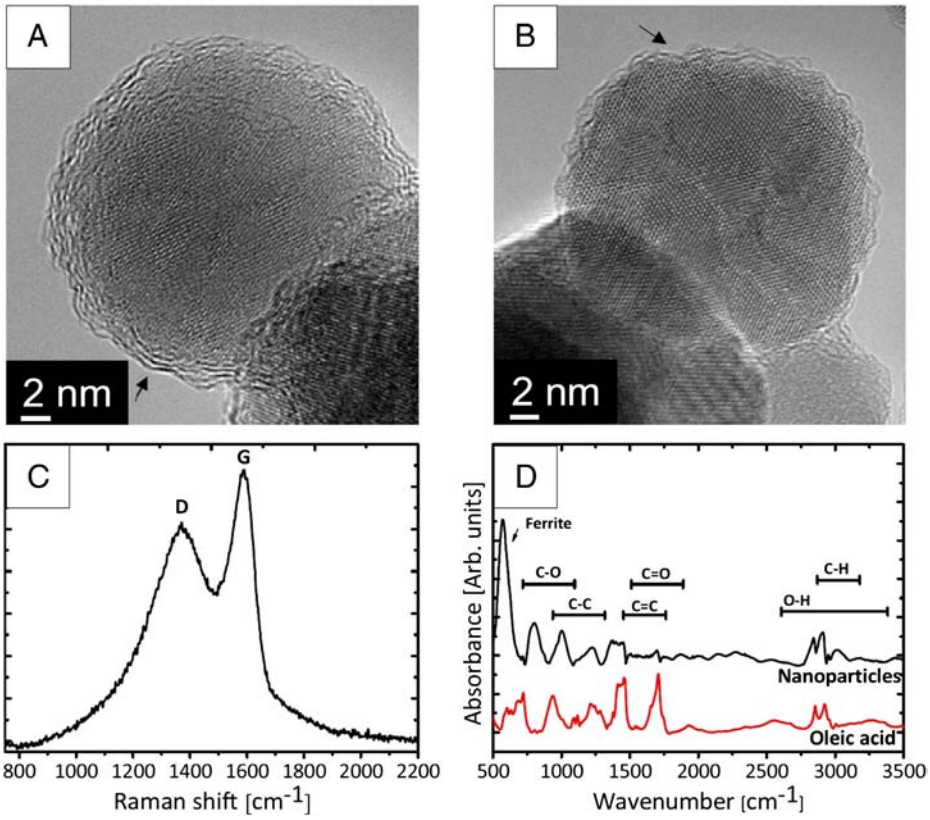

Fig. 2. TEM images with arrows highlighting the graphitic coating are shown in (A) and (B). In (C) the Raman spectra show the presence of D and G modes confirming the presence of sp^2 carbon. In (D) the infrared spectroscopy indicates the presence of functional groups.

The crystalline structure of the samples was studied using X-ray diffraction (XRD). Typical XRD patterns are provided in Fig. 3A. From the XRD data the average crystal size can be estimated according to the Scherrer equation [41]

$$D_{hkl} = \frac{K.\lambda}{\beta.\cos(\theta)}, \quad (1)$$

where K is a shape constant factor (for spherical NPs K = 0.9), λ is the X-ray wavelength (1.546 Å), β is the full width at half maximum (FWHM) expressed in units of 2θ (radians) and θ is the Bragg angle (in radians). The average crystal diameter (D_{hkl}) for each sample was calculated and is shown in Table 1. The values are in good agreement with the average particle size determined in the LVTEM investigations.

Analysis of the lattice spacing values does not provide sufficient information to differentiate between the magnetite (Fe_3O_4) and maghemite (γ-Fe_2O_3) phases since their signature peak positions are very similar. The use of Mössbauer spectroscopy can differentiate between the NP phases. It is however important to mention that the NPs used are carbon-coated so that in terms of surface interaction with the environment the phase of the nanoparticle is of minor relevance. Nonetheless the NP phase was indirectly probed using a simple method described by Sun and Zeng [42] to differentiate between the magnetite and maghemite phases.

The technique relies upon the fact than when annealing in air magnetite converts to the hematite (α-Fe_2O_3) phase whereas the maghemite phase does not change. Since the XRD pattern of hematite is very distinct from the other iron oxide phases the annealing process helps to identify the presence of magnetite. The result of the annealing process is shown in Fig. 3B. The XRD reflexes clearly show that the diffraction patterns of samples with diameters of 9.7 and 14.8 nm have new peaks characteristic of the hematite phase at the crystalline coordinates (104), (113), (024), (116), and (300), while the XRD reflexes of the samples with 16.8 and 20.3 nm remain unaltered. The data suggests that these two samples with smaller mean diameters are mostly composed of magnetite, while the two samples with larger mean diameters comprise the maghemite phase. This finding follows an opposing trend to that found by Park et al. [37], who observed an increase in magnetite content

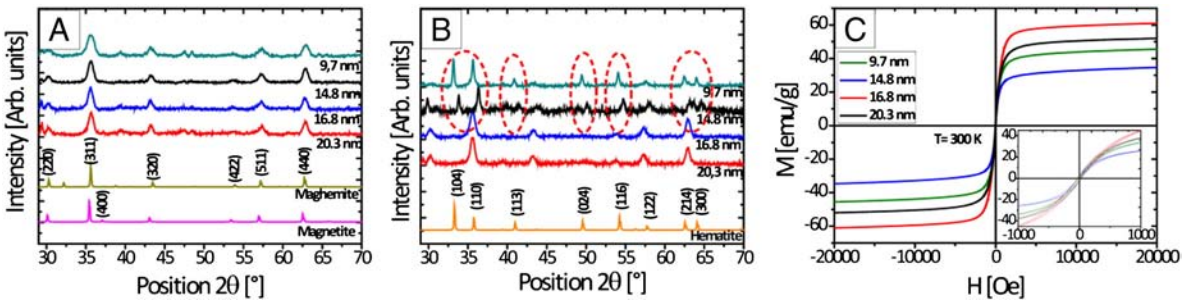

Fig. 3. XRD reflexes before and after annealing in air are shown in (A) and (B). In (C) the magnetization curves (at T = 300 K) are presented.

with increasing particle size. We attribute this difference to slight variations in some of our synthesis parameters such as the synthesis atmosphere and temperature (e.g. we did not use a rotary heating system). We also conducted magnetization studies (see panel C of Fig. 3). The hysteresis curves confirm that the NPs pursue a ferromagnetic nature, while the exact stoichiometry of the samples could not be calculated from the magnetization curves since the difference in the magnetization saturation (M_S) suggests either a mix of phases and/or presence of non-magnetic material, for example diamagnetic organic material concomitant with a carbon coating. In order to further study the magnetic properties field-cooled and zero field-cooled curves (MxT) were measured. Samples with 14.8, 16.8 and 20.3 nm show ferromagnetic behavior with a blocking temperature above room temperature. The sample containing the smallest diameter (9.7 nm) shows a blocking temperature below room temperature ($T_B = 39$ K) indicating superparamagnetic behavior (see Fig. S1 in the supporting information).

3.2. Cytotoxicity evaluation

The size dependent cytotoxicity of the carbon-coated iron oxide NPs was investigated. Four different cell lines (HeLa Kyoto, human osteosarcoma U2OS, fibroblasts (NIH 3T3) and macrophages (J7442)) were incubated with the NPs dispersed in water at three distinct concentrations (1, 10 and 100 μg/mL) for a period of 12 and 48 h. In order to quantify the toxicity of the different NPs two different approaches were used. First, the number of viable cells was measured with a colorimetric assay that is based on the reduction of yellow MTT (3-[4,5-dimethylthiazol-2-yl]-2,5-diphenyltetrazolium bromide) to purple formazan crystals by mitochondrial dehydrogenase enzymes. The cleavage of MTT occurs only in living cells so that the amount of the produced formazan crystals is proportional to the number of living cells. In addition, to exclude the possible influence of the NPs on the test results, cell-free tests were simultaneously conducted. No influence of the NPs alone was detected (data not shown).

The MTT assay does not provide any information as to whether the NPs themselves cause cell death or whether they simply reduce the cellular metabolic activity. Hence we implement a second approach, the dye exclusion method with trypan blue. The cell viability assay is based on the exclusion of the blue dye from healthy cells. In dead cells the membrane is no longer functional (ruptured) and the dye is able to cross the membrane, staining the cell interior. Using a visible light microscope, the dead cells are observed to be dark blue instead of bright.

3.2.1. Incubation for 12 h with cells

The MTT assay was first performed for an incubation period of 12 h. The data from the MTT assay of this short-exposure are provided in Fig. S2 in the supplementary information. The results suggest that it is not possible to relate the decrease in viability between the cell lines tested to the size of the NPs. The trypan blue test conducted for the short-exposure time (12 h) also demonstrates no change in viability as can be seen in Fig. S3 in the supplementary information. As with the MTT assay, no size dependence was observed in the trypan blue assay.

3.2.2. Incubation for 48 h with cells

In order to observe any time-dependent influence of toxicity, the MTT assay was measured for a long exposure time (48 h). This data shows slightly different values of cytotoxicity as compared to the short-exposure time. The MTT viability results for each cell line are provided in Fig. 4(A–D). For the four investigated cell lines the nanoparticle solutions with a concentration of 1 μg/mL did not show a toxic effect. For a NP concentration of 10 μg/mL there is a slight decrease in viability, which is more pronounced for the macrophage cell line (in Fig. 4D). With a NP concentration of 100 μg/mL all cell lines show an obvious decrease in viability. Both the human HeLa (Fig. 4A) and osteosarcoma (Fig. 4B) cell lines show a higher resistance to the NPs as compared to the mouse cell lines. This difference is most evident when comparing the NP solutions of 100 μg/mL. Despite the decrease in viability when compared to the short-exposure incubation periods, the data show no apparent size dependence or diameter distribution dependence on toxicity within the explored diameter range. The results suggest that the toxicity of the NPs is primarily defined by the nanoparticle concentration.

The dye exclusion test (trypan blue) was also conducted for the smallest and biggest NP diameters (9.7 and 20.3 nm). In Fig. 4E a typical light micrograph of the cells treated with the dye is shown. The arrows indicate blue and therefore dead cells. The results for all cell lines and a NP concentration of 10 μg/mL are shown in Fig. 4F. The HeLa, osteosarcoma (U2OS) and fibroblast (NIH 3 T3) cell lines do not exhibit a prominent change in viability, while the macrophages (J7442) do show a slight decrease in viability.

This decrease is however less than that observed in the MTT assay. This indicates that the cells incubated with the carbon-coated iron oxide NPs tend to undergo a reduction in mitochondrial activity (indicated by MTT assay) rather than die (as indicated by the trypan blue assay).

3.3. Cluster formation

In practice, some NPs will agglomerate due to magnetic interactions, and to a lesser degree through van der Waals interactions. Indeed visible light microscopy studies of the NPs confirm the presence of clusters in the NP solution. To investigate if there is a dependence of the cluster size on toxicity the MTT and trypan blue tests for the smallest and largest diameter samples (samples *a* and *d*) were repeated. For the new set of experiments, two cell lines were explored (HeLa Kyoto and macrophages) and the NP samples were sonicated in order to obtain a better dispersion of the NPs in the aqueous solution. The HeLa Kyoto cell line was chosen as a standard human cell line whose toxic response did not significantly differ from the osteosarcoma one and as a mouse cell line, the macrophages were chosen because they showed the highest sensitivity. Before incubating the NPs with these cells, the solutions were sonicated for 50 h to dissociate formed clusters. From visible light microscopy investigations the mean cluster size for the NPs with 9.7 nm was reduced by 70% and for the sample with NPs with 20.3 nm a 45% reduction was observed. It is also important to note that the same experiments with the sonicated samples were also conducted and in this case there was neither an increase nor a decrease in viability (see in Figs. S2 and S3 in the supplementary information). The data for the MTT and trypan blue studies are provided in Fig. 5. The MTT assay shows an increase in mitochondrial activity as compared to the non-sonicated samples initially investigated. This effect was more prominent for the macrophages. The increase in viability for the sonicated samples was more evident for the highest concentration of NPs used (100 μg/mL). These observations are in accordance with the trypan blue assay (see Fig. 5D). This difference is most probably assigned to the fact that the big clusters precipitate and accumulate on top of the cells, forming a rather large amount of material that eventually influences the cell proliferation. The samples with improved dispersion will have a larger number of small clusters and individual NPs that either do not precipitate or can be internalized and processed by cellular organelles. This leads to a relative increase in cellular activity as we observe. Transmission electron microscopy studies, discussed below, confirm that the cells do uptake individual NPs and small clusters as opposed to large clusters. This indicates that the carbon-coated iron oxide NPs are tolerated by cells even for large concentrations when the NPs are well dispersed or with small clusters.

3.4. Uptake studies

The uptake of the carbon-coated iron oxide NPs was investigated using visible light microscopy and TEM. The visible light microscopy studies were conducted for all four cell lines for the NP concentration of 10 μg/mL. Two representative snapshot images are provided in Fig. 6, panels A and B. The full videos showing a greater detail of the

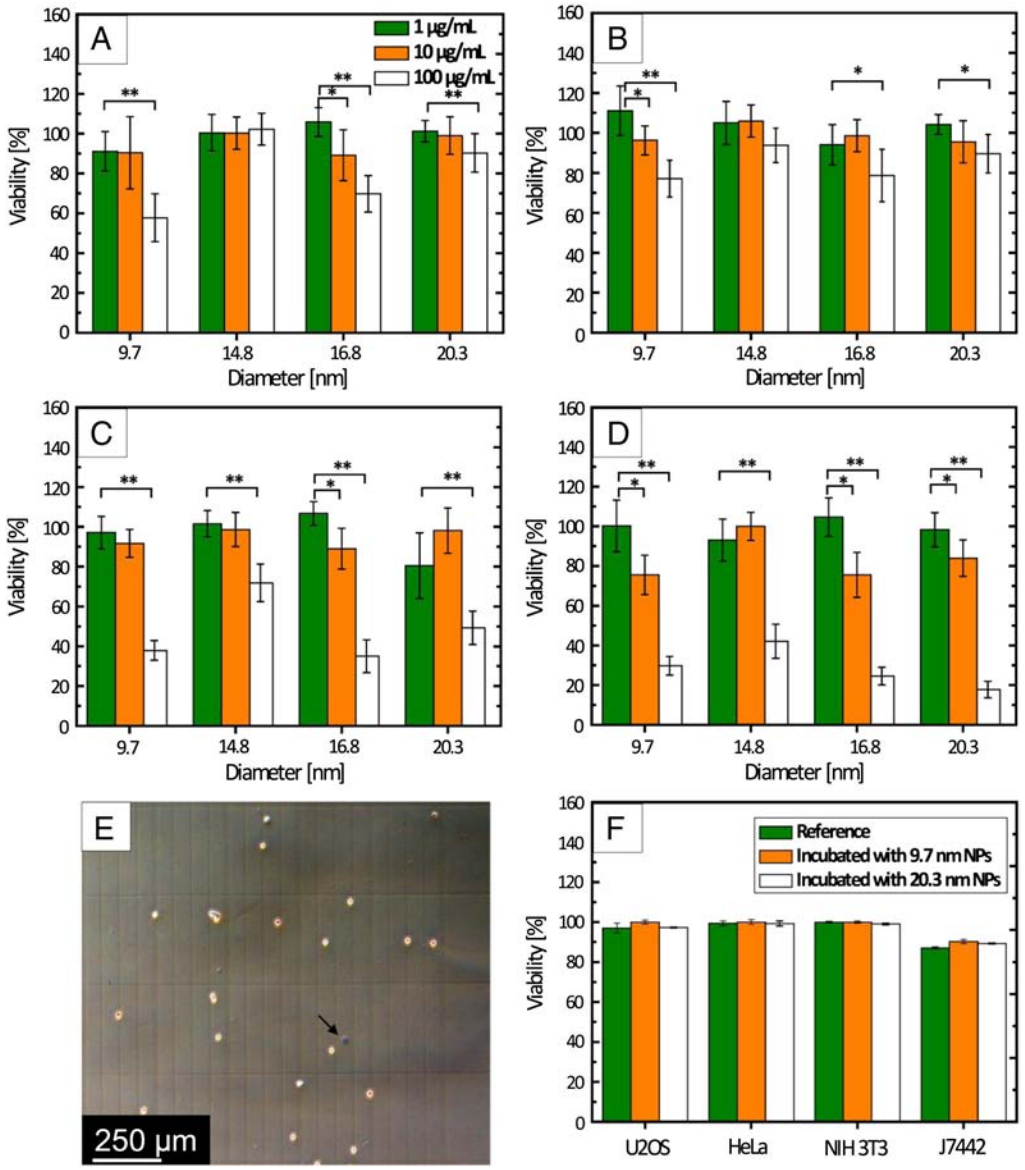

Fig. 4. Percentage viability of different cell lines in dependence on the nanoparticle diameter for three different nanoparticle concentrations using the MTT assay (green: 1 μg/mL, orange: 10 μg/mL, white: 100 μg/mL) for A) HeLa Kyoto, B) human osteosarcoma U2OS (GFP-53BP1), C) NIH 3T3 fibroblasts and D) Macrophages J7442. Error bars represent the standard deviation; *: $p < 0.05$ and **: $p < 0.001$. In panel E an example of a light micrograph image of the trypan blue viability assay is shown (the arrow indicates a dead cell) and in panel F the comparison of the percentage cell viability for the different cell lines for two nanoparticle diameters (green: untreated cells, orange: 10 nm Nanoparticle and white: 20 nm Nanoparticle 48 h incubation) is provided. The nanoparticle concentration in each case is 10 μg/mL.

cells in the presence of the NPs were recorded and provided in the supplementary information. The live observation of the cells incubated with NPs shows that they are able to carry large clusters that seem to be attached to their membrane. The cells however appear to continue their regular proliferation cycle (see videos and frames in the supplementary information). In addition, the macrophages tend to accumulate around the clusters, possibly in an attempt to conduct phagocytosis — a process in the natural immune response to remove pathogens and cell debris. To determine if the observed clusters were internalized, micrographs of different focal planes within the cells were taken and analyzed. The z-stacking of the images is shown in Fig. 6A and B. Unfortunately, although the NPs/clusters were obviously in contact with the cellular material, their internalization could not be fully resolved by this technique and thus the study was inconclusive. Hence, studies with TEM were conducted. The TEM analysis of the treated HeLa cells (Fig. 6C) and macrophages (Fig. 5D) shows that both cell lines internalize rather large amounts of NPs. In Fig. 6E a higher magnification image of the internalized NPs is distinguishable. Both small clusters (<100 nm) and individual NPs can be seen inside the endosome. No large clusters were ever observed within cells. Finally in Fig. 6F a high resolution image of an individual carbon-coated iron oxide NP is presented. The lattice structure of the particle is easily observable. Moreover, the TEM investigations of the uptake suggest that cells can indeed discriminate between the sizes of two of the samples investigated: the data strongly suggests that the 9.7 nm NPs, for both the HeLa cells and macrophages, are hardly internalized after the 12 h incubation, whereas the 20.3 nm NPs are seen to be internalized in large numbers by both cells. In order to improve our understanding in the NP internalization, further experiments to test the uptake were conducted for the 24 h incubation and a similar trend is observed in that significantly fewer particles of the 9.7 nm NPs were internalized as compared to the larger ones. However, after 48 h this difference is less distinct. It is important to point out that the characterization data shows that all samples are identical in all respects except diameter, this data strongly suggests that cells are indeed able to discriminate between small size differences of NPs. The reason for the difference is still not clear and

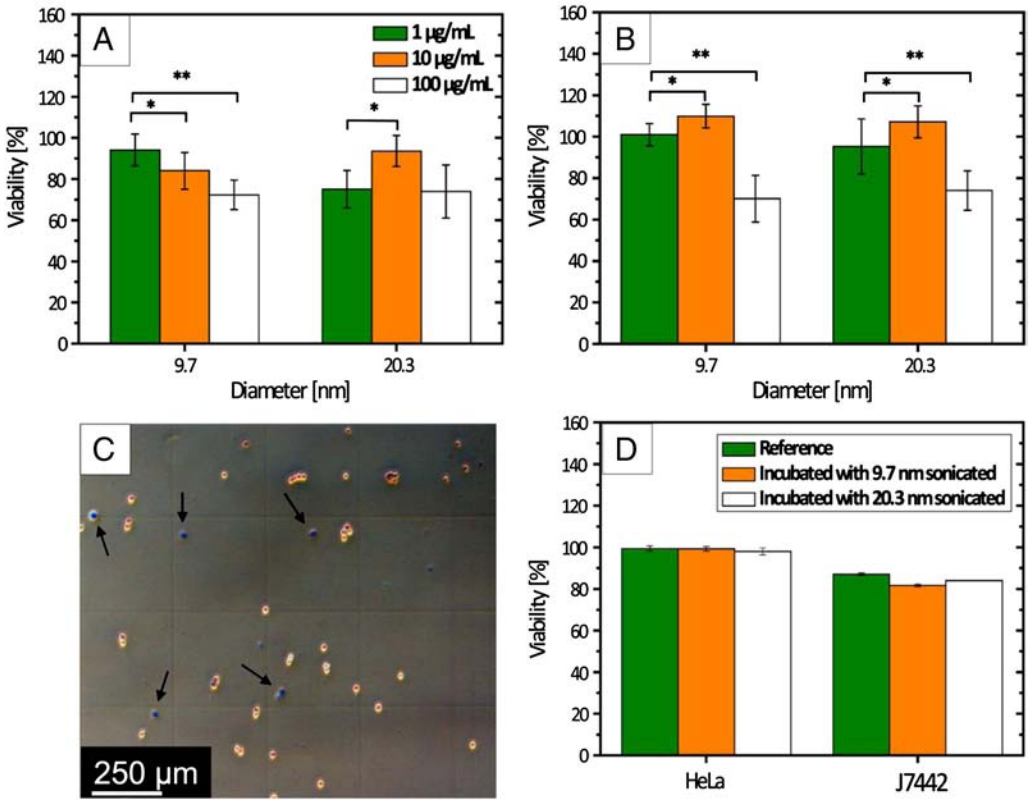

Fig. 5. Panels A and B show the MTT assay conducted with the HeLa and macrophages for the sonicated nano-particles with the smallest (9.7 nm) and biggest size (20.3 nm) diameter. The experiment was performed for different concentrations (green: 1 μg/mL, orange: 10 μg/mL and white: 100 μg/mL). This assay with the sonicated nano-particles shows an increase in cell viability in comparison to our initial tests. Panel D shows an example of the cells treated with the trypan blue — the arrows indicate dead cells. Panel D shows the results for the two cell lines treated with the nano-particles.

needs to be further investigated in future studies. Representative TEM images of the uptake studies are provided in Figs. S5 and S6 in the supplementary information.

4. Discussion

When comparing our results with work from others it becomes apparent that there seem to be differences between not only our samples but also between those from different research groups as a whole. For example, according to the obtained results the mouse fibroblasts show no or low cytotoxicity effects when incubated with the NPs at a concentration between 1 and 10 μg/mL, whereas relatively high toxic effects are observed for concentrations of 100 μg/mL. Other studies using mouse fibroblast cells show no toxicity even at 500 μg/mL [43–45]. Another study evaluating the toxicity of superparamagnetic iron oxide nanoparticles (SPIONs) on a human lung epithelial cell line showed low toxicity for these particles in concentrations raging from 20 to 80 μg/mL. Others found high toxicity levels at the same concentration on human fibroblast [46,47]. This indicates that the cytotoxicity of iron oxide NPs is dependent on multiple parameters. The presented study here in which a set of three narrow diameter distribution samples and a broader diameter distribution sample were investigated show little difference between all four NP samples. This indicates, that to some extent broad diameter distributions (as used in studies by others) are unlikely the reason behind the discrepancies. Our data show that the presence of clusters can affect cytotoxicity evaluations. Opposite to the cytotoxicity tests, the uptake studies indicate a strong difference in internalization for diameters between the 9.7 and 20.3 nm mean diameter samples. Moreover, TEM investigations indicate that cells uptake both individual particles and smaller clusters. In our four cell line study, some differences between cell lines were observed, and this highlights that toxicity variations can exist between different cell lines. Studies by Ying and Hwang [16] found that while the nanoparticle size (10 and 50 nm) shows little effect on toxicity, the surface coating can significantly alter cytotoxicity results. In short, determining the cytotoxicity effects of iron oxide NPs is complex.

5. Conclusions

Carbon-coated iron oxide NPs with three well-defined diameter distributions and a fourth sample with a broad diameter distribution spanning the range of the first three samples were synthesized and thoroughly characterized. Cytotoxicity evaluations of these samples showed no apparent difference between them; however, cluster formation was able to alter cytotoxicity results, albeit to a limited degree. In other words, it is not possible to observe changes in cell viability within a small NP diameter range (10 nm), suggesting that samples containing NPs with a broader diameter distribution are suitable for conducting cytotoxicity evaluations, since the narrow distribution results presented similar values of viability. Surprisingly, clear differences in particle uptake were observed with respect to the particles mean diameter sizes. The preferential uptake of NPs in cells depending on particle size is very important because it suggests that the morphology of NPs can already be used to trigger biological responses (in this case cellular uptake). This knowledge might prove promising in tailored responses of cells for biomedical applications.

Supplementary data to this article can be found online at http://dx.doi.org/10.1016/j.bbagen.2013.08.025.

Acknowledgements

RGM thanks the DFG (RU1540/8-1). BK, SS and OGS acknowledge Volkswagen Foundation for funding via project number 86 362. AAE acknowledges funding by the Egyptian government via Grant No. 2/2/66/

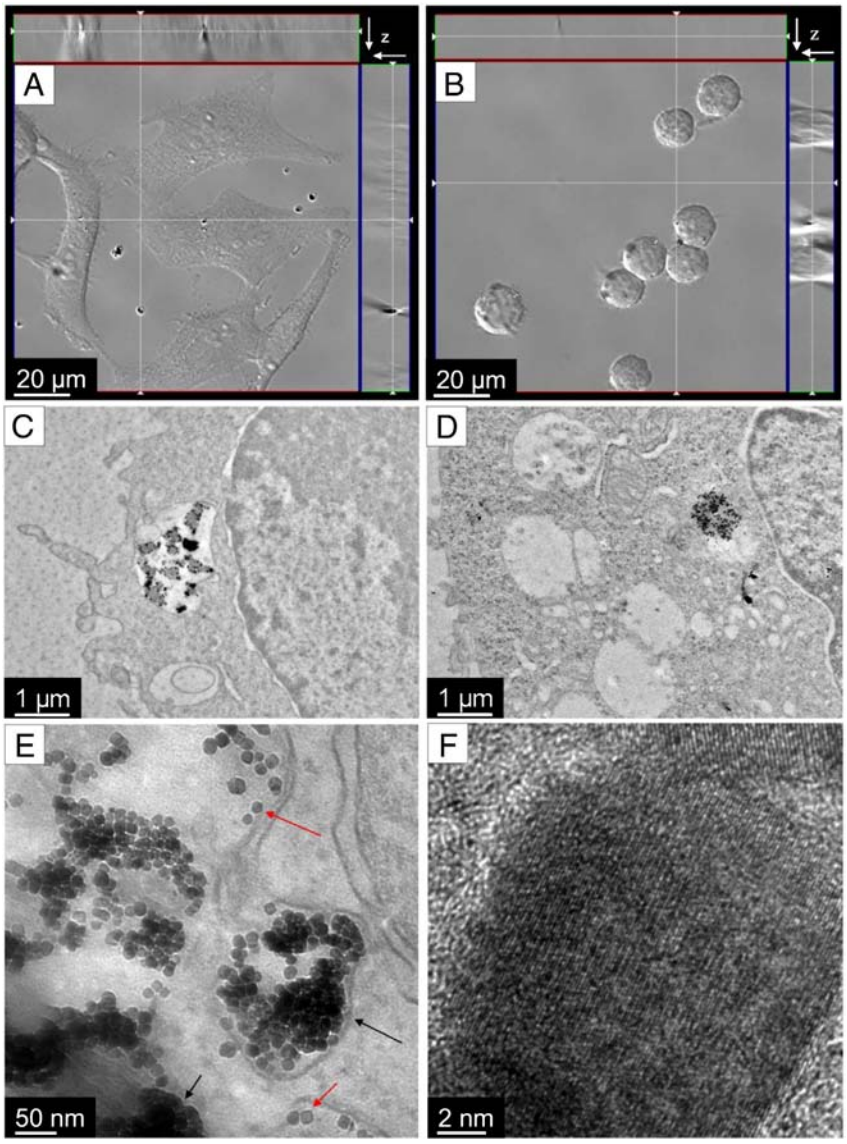

Fig. 6. Light micrographs (z-stacks) of A) HeLa Kyoto and B) Macrophage J7442 cells cultured in the presence of a 10 μg/mL nanoparticle dispersion (diameter 9.7 nm) after an incubation period of 48 h. The white lines indicate the cut views through each z-stack that are displayed at the top and right side of the pointed focal plane. In panels C, D and E TEM micrographs of the HeLa and Macrophages show that the incubated cells take up particles and small clusters. In panel F a high magnification image of a nano-particle showing the crystalline structure inside a cell is presented.

2005. MHR and BA thank the Institute for Basic Science (IBS) Korea for support. MHR also thanks the EU (ECEMP) and the Freistaat Sachsen. The HeLa and U2OS cell lines were kindly provided by Dr. Christine Schmidt, Wellcome Trust/Cancer Research UK Gurdon Institute, Cambridge.

References

[1] M.K. Yu, Y.Y. Jeong, J. Park, S. Park, J.W. Kim, J.J. Min, K. Kim, S. Jon, Drug-loaded superparamagnetic iron oxide nanoparticles for combined imaging and therapy in vivo, Angew. Chem. Int. 47 (2008) 5362–5365.
[2] C.T. Yavuz, J.T. Mayo, W.W. Yu, A. Prakash, J.C. Falkner, S. Yean, L. Cong, H.J. Shipley, A. Kan, M. Tomson, D. Natelson, V. Colvin, Low-field magnetic separation of monodisperse Fe_3O_4 nanocrystals, Science 314 (2006) 964–967.
[3] R. Weissleder, A. Bogdanov, E.A. Neuwelt, M. Papisov, Long-circulating iron oxides for MR imaging, Adv. Drug Deliv. Rev. 16 (1995) 321–334.
[4] C. Chouly, D. Pouliquen, I. Lucet, J.J. Jeune, P. Jallet, Development of superparamagnetic nanoparticles for MRI: effect of particle size, charge and surface nature on biodistribution, J. Microencapsul. 13 (1996) 245–255.
[5] B. Thiesen, A. Jordan, Clinical applications of magnetic nano-particles for hyperthermia, Int. J. Hyperthermia 24 (2008) 467–474.
[6] P. Reimer, R. Weissleder, Development and experimental application of receptor-specific MR contrast media, Radiology 36 (1996) 153–163.
[7] P.K. Gupta, C.T. Hung, Magnetically controlled targeted microcarrier systems, Life Sci. 44 (1989) 175–186.
[8] W. Jiang, B.Y.S. Kim, J.T. Rutka, W.C.W. Chan, Nanoparticle-mediated cellular response is size-dependent, Nat. Nanotechnol. 3 (2008) 145–150.
[9] L.C. Stoehr, E. Gonzalez, A. Stampfl, E. Casals, A. Duschl, V. Puntes, G.J. Oostingh, Shape matters: effects of silver nanospheres and wires on human alveolar epithelial cells, Part. Fibre Toxicol. 8 (2011) 1–15.
[10] X. Huang, X. Teng, D. Chen, F. Tang, J. He, The effect of the shape of mesoporous silica nanoparticles on cellular uptake and cell function, Biomaterials 31 (2010) 438–448.
[11] B.D. Chithrani, A.A. Ghazani, W.C. Chan, Determining the size and shape dependence of gold nanoparticle uptake into mammalian cells, Nano Lett. 6 (2006) 662–668.
[12] T.H. Chung, S.H. Wu, M. Yao, C.W. Lu, Y.S. Lin, Y. Hung, C.Y. Mou, Y.C. Chen, D.M. Huang, The effect of surface charge on the uptake and biological function of mesoporous silica nanoparticles in 3T3-L1 cells and human mesenchymal stem cells, Biomaterials 28 (2007) 2959–2966.
[13] S.E.A. Gratton, P.A. Ropp, P.D. Pohlhaus, J.C. Luft, V.J. Madden, M.E. Napier, J.M. DeSimone, The effect of particle design on cellular internalization pathways, Proc. Natl. Acad. Sci. U. S. A. 105 (2008) 11613–11618.
[14] J.A. Champion, S. Mitragotri, Role of target geometry in phagocytosis, Proc. Natl. Acad. Sci. U. S. A. 103 (2006) 4930–4934.
[15] J. Meng, J. Fan, G. Galiana, R.T. Branca, P.L. Clasen, S. Ma, J. Zhou, C. Leuschner, C.S.S.R. Kumar, J. Hormes, T. Otiti, A.C. Beye, M.P. Harmer, C.J. Kiely, W. Warren, M.P. Haataja, W.O. Soboyejo, LHRH-functionalized superparamagnetic iron oxide nano-particles for breast cancer targeting and contrast enhancement, Mater. Sci. Eng. C 29 (2009) 1467–1479.

[16] E. Ying, H.M. Hwang, In vitro evaluation of cytotoxicity of iron oxide nano-particles with different coating and different sizes in A3 human T lymphocytes, Sci. Total Environ. 408 (2010) 4475–4481.
[17] H.L. Karlsson, J. Gustafsson, P. Cronholm, L. Möller, Size-dependent toxicity of metal oxide particles — a comparison between nano- and micrometer size, Toxicol. Lett. 188 (2009) 112–118.
[18] D. Hellstern, K. Schulze, B. Schöpf, A. Petri-Fink, B. Steitz, S. Kamau, M. Hilbe, S. Koch-Schneidemann, L. Vaughan, M. Hottiger, M. Hofmann, B. von Rechenberg, Systemic distribution and elimination of plain and with Cy3.5 functionalized poly(vinyl alcohol) coated superparamagnetic maghemite nanoparticles after intraarticular injection in sheep in vivo, J. Nanosci. Nanotechnol. 6 (2006) 3261–3268.
[19] B. Faddel, A.E. Garcia-Bennett, Better safe than sorry: understanding the toxicological properties of inorganic nanoparticles manufactured for biomedical applications, Adv. Drug Deliv. Rev. 62 (2010) 362–374.
[20] R. Mout, D.F. Moyano, S. Rana, V.M. Rotello, Surface functionalization of nanoparticles for nanomedicine, Chem. Soc. Rev. 41 (2012) 2539–2544.
[21] K.G. Neoh, E.T. Kang, Functionalization of inorganic nano-particles with polymers for stealth biomedical applications, Polym. Chem. 2 (2011) 747–759.
[22] A.S. Karakoti, S. Das, S. Thevuthasan, S. Seal, PEGylated inorganic nano-particles, Angew. Chem. Int. 50 (2011) 1980–1994.
[23] S. Park, H. Kim, W.J. Kim, H.S. Yoo, Pluronic@Fe_3O_4 nano-particles with robust incorporation of doxorubicin by thermo-responsiveness, Int. J. Pharm. 424 (2012) 107–114.
[24] A. Garcia-Bennett, M. Nees, B. Faddel, In search of the Holy Grail: folate-targeted nano-particles for cancer therapy, Biochem. Pharmacol. 81 (2011) 976–984.
[25] N.G. Bastús, E. Sánchez-Tilló, S. Pujals, S.C. Farrera, C. López, E. Giralt, A. Celada, J. Lloberas, V. Puntes, Homogeneous conjugation of peptides onto gold nano-particles enhances macrophage response, ACS Nano 3 (2009) 1335–1344.
[26] I. Ojea-Jiménez, L. García-Fernández, J. Lorenzo, V. Puntes, Facile preparation of cationic gold nanoparticle-bioconjugates for cell penetration and nuclear targeting, ACS Nano (2012), http://dx.doi.org/10.1021/nn3012042.
[27] Y. Saito, Nano-particles and filled nanocapsules, Carbon 33 (1995) 979–988.
[28] N. Junichi, O. Chie, O. Osamu, N. Nobuyuki, Synthesis, structures and magnetic properties of carbon-encapsulated nano-particles via thermal decomposition of metal acetylide, Carbon 44 (2006) 2943–2949.
[29] A. Taylor, Y. Krupskaya, S. Costa, S. Oswald, K. Krämer, S. Füssel, R. Klingeler, B. Büchner, E. Borowiak-Palen, M.P. Wirth, Functionalization of carbon encapsulated iron nano-particles, J. Nanopart. Res. 12 (2010) 513–519.
[30] A. Bonanni, A. Ambrosi, M. Pumera, On oxygen-containing groups in chemically modified graphene, Chem. Eur. J. 18 (2012) 4541–4548.
[31] L. Zhang, R. He, H.C. Gu, Oleic acid coating on the monodisperse magnetite nano-particles, Appl. Surf. Sci. 253 (2006) 302611–302617.
[32] M. Pumera, Carbon nanotubes and nano-particles in cell, Curr. Drug Metab. 13 (2012) 251–256.
[33] P. Lukanov, V.K. Anuganti, Y. Krupskaya, A. Galibert, B. Soula, C. Tilmaciu, A.H. Velders, R. Klingeler, B. Büchner, E. Flahaut, CCVD synthesis of carbon-encapsulated cobalt nano-particles for biomedical applications, Adv. Funct. Mater. 21 (2011) 3583–3588.
[34] Z. Liu, J.T. Robinson, X. Sun, H. Dai, PEGylated nanographene oxide for delivery of water-insoluble cancer drugs, J. Am. Chem. Soc. 130 (2008) 10876–10877.
[35] R. Klingeler, S. Hampel, B. Büchner, Carbon nanotube based biomedical agents for heating, temperature sensoring and drug delivery, Int. J. Hyperthermia 24 (2008) 496–505.
[36] A. Bonanni, A. Ambrosi, M. Pumera, Nucleic acid functionalized graphene for biosensing, Chem. Eur. J. 18 (2012) 1668–1673.
[37] J. Park, K. An, J.G. Park, H.J. Noh, J.Y. Kim, J.H. Par, N.M. Hwang, T. Hyeon, Ultra-large-scale syntheses of monodisperse nanocrystals, Nat. Mater. 3 (2004) 891–895.
[38] L.M. Bronstein, X. Huang, J. Retrum, S. Schmucker, M. Pink, B.D. Stein, B. Dragnea, Influence of iron oleate complex structure on iron oxide nanoparticle formation, Chem. Mater. 19 (2007) 3624–3632.
[39] A.C. Ferrari, Raman spectroscopy of graphene and graphite: disorder, electron–phonon coupling, doping and nonadiabatic effects, Solid State Commun. 143 (2007) 47–57.
[40] Z.P. Chen, Z. Xu, Y. Zhang, N. Gu, Effects of proteins from culture medium on surface property of silanes—functionalized magnetic nanoparticles, Nanoscale Res. Lett. 4 (2009) 204–209.
[41] A.L. Patterson, The Scherrer formula for X-ray particle size determination, Phys. Rev. 56 (1939) 978–982.
[42] S. Sun, H.S. Zeng, Size-controlled synthesis of magnetite nano-particles, J. Am. Chem. Soc. 124 (2002) 8204–8205.
[43] M. Mahmoudi, M.A. Shokrgozar, A. Simchi, M. Imani, A.S. Milani, P. Stroeve, H. Vali, U.O. Hafeli, S. Bonakdar, Cytotoxicity of uncoated and polyvinyl alcohol coated superparamagnetic iron oxide nanoparticles, J. Phys. Chem. C 113 (2009) 2322–2331.
[44] M. Mahmoudi, A. Simchi, M. Imani, Cytotoxicity of uncoated and polyvinyl alcohol coated superparamagnetic iron oxide nanoparticles, J. Phys. Chem. C 113 (2009) 9573–9580.
[45] M. Mahmoudi, A. Simchi, H. Vali, M. Imani, M.A. Shokrgozar, K. Azadmanesh, F. Azari, Cytotoxicity and cell cycle effects of bare and polyvinyl alcohol coated iron oxide nanoparticles in mouse fibroblasts, Adv. Eng. Mater. 11 (2009) B243–B250.
[46] A.K. Gupta, C. Berry, M. Gupta, A. Curtis, Receptor-mediated targeting of magnetic nanoparticles using insulin as a surface ligand to prevent endocytosis, IEEE Trans. Nanobioscience 2 (2003) 256–261.
[47] A.K. Gupta, S. Wells, Surface-modified superparamagnetic nano-particles for drug delivery: preparation, characterization, and cytotoxicity studies, IEEE Trans. Nanobioscience 3 (2004) 66–73.